DFT and In Situ EXAFS Investigation of Gold/Ceria−Zirconia Low-Temperature Water Gas Shift Catalysts: Identification of the Nature of the Active Form of Gold

D. Tibiletti,[†] A. Amieiro-Fonseca,[‡] R. Burch,[†] Y. Chen,[†] J. M. Fisher,[‡] A. Goguet,[†] C. Hardacre,*[,†] P. Hu,[†] and D. Thompsett[‡]

CenTACat and School of Chemistry and Chemical Engineering, Queen's University Belfast, Belfast BT9 5AG, Northern Ireland, U.K., and Johnson Matthey Technology Centre, Blounts Court, Sonning Common, Reading RG4 9NH, U.K.

Received: August 15, 2005; In Final Form: September 27, 2005

A combined experimental and theoretical investigation of the nature of the active form of gold in oxide-supported gold catalysts for the water gas shift reaction has been performed. In situ extended X-ray absorption fine structure (EXAFS) and X-ray absorption near-edge structure (XANES) experiments have shown that in the fresh catalysts the gold is in the form of highly dispersed gold ions. However, under water gas shift reaction conditions, even at temperatures as low as 100 °C, the evidence from EXAFS and XANES is only consistent with rapid, and essentially complete, reduction of the gold to form metallic clusters containing about 50 atoms. The presence of Au−Ce distances in the EXAFS spectra, and the fact that about 15% of the gold atoms can be reoxidized after exposure to air at 150 °C, is indicative of a close interaction between a fraction (ca. 15%) of the gold atoms and the oxide support. Density functional theory (DFT) calculations are entirely consistent with this model and suggest that an important aspect of the active and stable form of gold under water gas shift reaction conditions is the location of a partially oxidized gold ($Au^{\delta+}$) species at a cerium cation vacancy in the surface of the oxide support. It is found that even with a low loading gold catalysts (0.2%) the fraction of ionic gold under water gas shift conditions is below the limit of detection by XANES (<5%). It is concluded that under water gas shift reaction conditions the active form of gold comprises small *metallic* gold clusters in intimate contact with the oxide support.

Introduction

Nanoparticles of gold supported on metal oxides have been shown to be very active for several reactions such as CO oxidation or low-temperature water gas shift (WGS).[1−8] The catalysis of the WGS reaction over supported gold catalysts has recently been the subject of numerous investigations. This reaction is a key step in applications such as on-board H_2 production via reforming processes for fuel cell applications. In such applications, a successful low-temperature WGS catalyst will have to possess high activity as well as good structural stability under all reaction conditions. However, existing catalysts do not meet these stability requirements, and many research programs have been undertaken in order to discover more stable and more active catalysts.

The early work in this area focused on Au/Fe_2O_3 catalysts.[9−19] The activity of these iron oxide-based catalysts was reported to exceed that of the state-of-the-art $CuO/ZnO/Al_2O_3$ low-temperature WGS catalyst. Since then a wide range of supported gold catalysts have been examined, including those based on TiO_2,[20−24] ZnO,[18] ZrO_2,[18] NaY,[25] Na−mordenite,[25] and Na−ZSM-5[25] with the Fe_2O_3 and TiO_2 catalysts found to be the most active. However, the stability of Au/Fe_2O_3 catalysts, in particular, is limited due to agglomeration of the gold. This is probably related to a reduction in total surface area on transforming γ-Fe_2O_3 to α-Fe_2O_3 and Fe_3O_4.[26] More recently, CeO_2 and doped CeO_2 supported gold catalysts have been studied for WGS conditions in order to improve their activity and stability.[27−32] Recent results on gold supported on La- or Gd-doped CeO_2,[27,33−35] CeO_2 promoted with various elements (Co, Fe, Ni, Pt, Cu),[36] and very recently $CeZrO_x$[37] have displayed promising results showing that these supported gold catalysts are very active for the WGS reaction and generally more stable than catalysts supported on Fe_2O_3.

It is also evident, that regardless of the support, the method of introducing Au onto the support is crucially important for the resultant activity of the catalyst.[13,24,38] The preparation is critical if the gold−support interaction is to be effective and if a suitable metal particle size distribution is to be obtained. Although it has been established that nanosized particles of gold supported on reducible oxides are remarkably active for a whole variety of different reactions, there is very little consensus on the specific characteristics of the supported gold responsible for the high activity. This lack of agreement is particularly striking for ceria-supported gold catalysts used for the WGS reaction.

Fu et al.[27,34,35] examined the metal/support interaction in gold supported on calcined ceria, and La- or Gd-doped ceria catalysts, prepared via deposition−precipitation. Both the fresh and NaCN leached catalysts were found to exhibit similar WGS reaction rates. X-ray photoelectron spectroscopy (XPS) characterization showed that Au^0, Au^+, and Au^{3+} were present in the parent catalysts, while the leached samples contained only ionic gold. Furthermore, cationic gold was found in all gold ceria samples prepared by various techniques and after use in the WGS environment for many hours. X-ray diffraction (XRD) charac-

* To whom correspondence should be addressed. E-mail: c.hardacre@qub.ac.uk.
[†] Queen's University Belfast.
[‡] Johnson Matthey Technology Centre.

10.1021/jp054576s CCC: $30.25
Published on Web 11/09/2005

terization showed that the deposition of gold caused a perturbation of the lattice constant of the support and that this perturbation was similar for both the parent and leached samples. Interestingly, Venezia et al.[39] also reported that gold perturbed the ceria lattice and attributed the shifts as due to Au^{+} and Au^{3+}, replacing Ce^{4+} in the lattice. Fu et al.[27,34,35] concluded that metal gold nanoparticles do not participate in the water gas shift reaction, but rather that the active site for WGS reaction was cationic gold bound strongly in the ceria surface. The diffusion of Au ions into the ceria is proposed to take place during the heating step in the preparation process or thermal treatment in the reformate type gas mixture. However, Fu et al. also note that the XP spectra of the samples showed that the oxidation state of the gold changed with reaction conditions. In more oxidizing atmospheres, ionic gold is clearly seen in the used sample, while, in more reducing atmospheres, the peaks of Au became sharper and gold particle growth was measured.

In contrast, Tabakova et al.[30,32] have used in situ FTIR on Au/CeO_2 catalysts to observe a strong band at 2060 cm^{-1} on the freshly reduced catalyst. This band was attributed to CO adsorbed on small negatively charged gold clusters of various sizes. Following the WGS reaction the gold had zero charge as indicated by the CO IR absorption peak at 2094 cm^{-1}. On the basis of those observations, it was speculated that as the catalyst was exposed to the WGS mixture, CO would be adsorbed mainly on $Au^{\delta-}$ sites, which in the presence of water would become Au^0 or $Au^{\delta+}$. As a consequence of water dissociation on ceria vacancies in close contact with gold clusters, the hydrogen thus produced could reduce again the catalyst under working conditions. The high stability of this catalyst prepared by deposition−precipitation of the gold was attributed to resistance to sintering of the small gold clusters in intimate contact with the ceria. Therefore, the reaction was proposed to proceed at the boundary between small metallic gold particles and ceria, where CO adsorption on gold and H_2O dissociation on ceria defects could take place.

The present paper reports on the use of in situ extended X-ray absorption fine structure (EXAFS) coupled with density functional theory (DFT) calculations to elucidate the structure of highly active $Au/CeZrO_4$ catalysts for WGS. The transformation as a function of reaction conditions is described, and the relationship between the structure of the catalyst in active and deactivated forms is found to support a model based on small *metallic* gold particles in intimate contact with the support.

Experimental Section

Catalyst Preparation. Catalysts prepared by the following general route (using 2% $Au/CeZrO_4$ to illustrate). $CeZrO_4$ (Rhodia, 19.6 g) was slurried in water (800 cm^3) and warmed to 60 °C. The pH was adjusted to 8.0 by the addition of sodium carbonate (0.05 M). $HAuCl_4$ (0.81 g, 49.24% Au) was dissolved in water (150 cm^3) and pumped into the stirred support slurry at ca. 10 cm^3 min^{-1}. The pH was monitored throughout and base (0.05 M Na_2CO_3) was pumped in at variable rate to maintain the pH as close as possible to 8.0 throughout the gold addition. This was achieved using a three-term proportional-integral derivative (PID) controller with feedback loop to the pH probe. After the gold addition was complete, stirring was continued for a further 1 h. The catalyst sample was recovered by filtration, thoroughly washed to remove soluble chloride, and oven dried at 105 °C for 16 h. The final catalyst had a gold content of 1.7%. For the CeO_2 and TiO_2 catalysts, an equivalent procedure was employed using CeO_2 (Rhodia) and TiO_2 (Millenium Chemicals).

Activity Tests. The activity of the catalyst for the water gas shift reaction was tested in an apparatus, detailed elsewhere.[40] The gases (H_2, N_2, CO, and CO_2, supplied by BOC) were >99.9% purity and used without further purification. The steam was fed by saturating the mixture of gases with water. The gases were passed through a water saturator, where the temperature was controlled by a Grant LTD6G thermostatic bath. Then the mixture of gases was flowed through the reactor or through the bypass. The reactor consisted of a 28 cm length quartz tube, with internal diameter of 5 mm. The catalyst bed was held between two plugs of quartz wool. The temperature in the reactor was controlled by a Eurotherm 2604. The analysis of the gases coming from the reactor/bypass was carried out by employing a Perkin-Elmer Clarus 500 gas chromatograph fitted with a Hayesep N (80-100) column. The water and the hydrogen were analyzed by a thermal conductivity detector (TCD), while carbon monoxide, methane, and carbon dioxide were analyzed both by the TCD and by a flame ionization detector (FID) fitted with a methanator. The temperatures inside the water saturator, into the reactor and along the pipe-line before and after the furnace, were measured by type K thermocouples, recorded by a Pico Technology Ltd. TC-08 box, and the data were stored in a personal computer.

Typically 150 mg of catalyst was loaded in the reactor and exposed to the WGS mixture (2.0% CO, 2.5% CO_2, 7.5% H_2O, and 8.1% H_2 in N_2) at 100 °C without any pretreatment (Gas Hourly Space Velocity, GHSV = 40 L g^{-1} h^{-1}). The temperature of the reactor was increased to the desired set point using a 1 °C min^{-1} temperature ramp, while the concentrations of the gases (CO, CO_2, H_2O, and H_2) were monitored by gas chromatography.

Deactivation studies were also performed under the same WGS conditions reported above. The temperature of the catalyst bed was raised from 100 °C to either 250 or 350 °C at 1 °C min^{-1}, held at the desired temperature for 20 min, and then lowered to 100 °C in the WGS mixture. Subsequently, the temperature was raised (4 °C min^{-1}) in the WGS mixture in order to investigate the stability of the catalyst.

In Situ EXAFS and XANES. Data were collected at the Synchrotron Radiation Source in Daresbury, U.K., using station 16.5. The fluorescence detection mode using a 32-channel Canberra solid-state detector. The spectra were recorded at the gold L_{III} edge using a double crystal Si(220) monochromator set at 50% harmonic rejection. Scans were collected and averaged using EXCALIB, which was also used to convert raw data into energy vs absorption data. EXBROOK was used to remove the background.

The analysis of the EXAFS was performed using EXCURV98[41] on the k^3-weighted raw data using the curved wave theory. Phase shifts were derived from ab initio calculations using Hedin−Lundqvist exchange potentials and von Barth ground states. Comparisons were made with reference Au foil, Au_2O_3, and $AuCl(PPh_3)_2$ powders. The in situ EXAFS and X-ray absorption near-edge structure (XANES) analysis were performed in a glass reaction cell with Kapton using a 20 mm diameter pressed pellet of catalyst supported in a stainless steel holder with the cell fixed to vertical and horizontal stepper motors. Typically, pellets of 50−100 mg of catalyst were used in order to minimize effects due to self-absorption. The temperature was controlled with a Eurotherm PID controller with a type K thermocouple in contact with the catalyst.

The EXAFS measurements obtained under WGS conditions were performed in a gas mix containing 2% CO, 2.5% CO_2, 8.1% H_2, and 7.5% H_2O. In all cases, the reactor was purged

TABLE 1: Calculated and Experimental Lattice Constants of CeO_2

	lattice constant/Å		lattice constant/Å
experiment[43a]	5.41	Yang et al.[44b]	5.45
this work	5.49	Liu et al.[45]	5.48
Skorodumovaetal. et al.[44a]	5.48		

TABLE 2: Calculated and Experimental Lattice Constants (a, c) of Ce_2O_3

	a/Å	c/a
experiment[43b]	3.888	1.55
this work	3.878	1.57
Liu et al.[45]	3.897	1.58

with helium prior to admitting the WGS mixture at 75 °C, whereon a small exotherm was observed on the catalyst of the order of 10−15 °C. At no stage did the catalyst temperature exceed 90 °C under these conditions. The catalysts were heated in the water gas shift mixture at temperatures up to 450 °C in the in situ cell; however, to obtain analyzable EXAFS data, the catalysts were cooled to 100 °C under the reacting atmosphere before the data were taken. A comparison of the data taken at the reaction temperature showed no significant change in the XANES or EXAFS with the exception of a decrease in the amplitude of oscillations due to increased thermal disorder. For the reoxidation treatment, the catalyst was purged with helium before slowly admitting the air in order to minimize any risk of exotherms. To reduce the risk of reduction of the catalyst in the X-ray beam, the sample was moved via the stepper motors after each scan limiting the number of scans possible for a given sample. Control experiments showed that photoelectron reduction of the sample was only detectable in the EXAFS after three consecutive scans with the sample at a static position.

DFT Calculation Details. The total energy calculations have been carried out using the SIESTA code[42a] based on the standard DFT-slab approach with the generalized gradients approximation (GGA) of Perdew−Bruke−Ernzerhof (PBE) functional and a double-ζ plus polarization basis set. Troullier−Martins norm-conserving pseudopotentials were used to describe the ionic cores. The energy cutoff for the real space grid used to represent the density was 180 Ry. The localization radii of the basis functions were determined from an energy shift of 0.01 eV. The cerium pseudopotential was fully tested, and some results are listed in Tables 1 and 2 for CeO_2 and Ce_2O_3, respectively. As can be seen, our calculated results are very close to the experimental values and previous DFT calculations.[43−45] For example, the error of our calculated lattice constant of CeO_2 is less than 1.5% compared to the experimental value. It should be stressed that one of the toughest tests is to calculate Ce_2O_3. The lattice constants from our calculations are similar to the values of the experiment and a recent DFT study. Perhaps more importantly, we checked the density of states in Ce_2O_3 and found that some f states of Ce are localized at the Fermi energy, which is consistent with experiments.

CeO_2(111) was modeled by a $p(2 \times 2)$ unit cell with nine layers in which the top three layers were relaxed, while CeO_2-(110) was modeled by a $p(2 \times 1)$ unit cell with five layers and the top layer relaxed.

Results

Activity Tests. Figure 1 shows the catalytic activity under WGS conditions for a range of oxide-supported Au catalysts and 2% Pt/CeO_2 catalyst as a reference catalyst. Among the catalysts investigated 2% $Au/CeZrO_4$ was the most promising

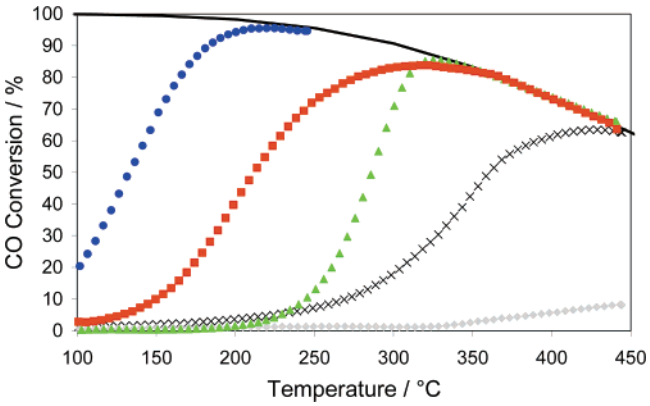

Figure 1. Catalytic activity under WGS conditions (2.0% CO, 2.5% CO_2, 7.5% H_2O, and 8.1% H_2 in N_2) for 2% $Au/CeZrO_4$ (blue filled circles), 0.2% $Au/CeZrO_4$ (red filled squares), 2% Au/CeO_2 (×), 2% Au/TiO_2 (gray filled diamonds), and 2% Pt/CeO_2 (green filled triangles). Full line shows the thermodynamic equilibrium conversion.

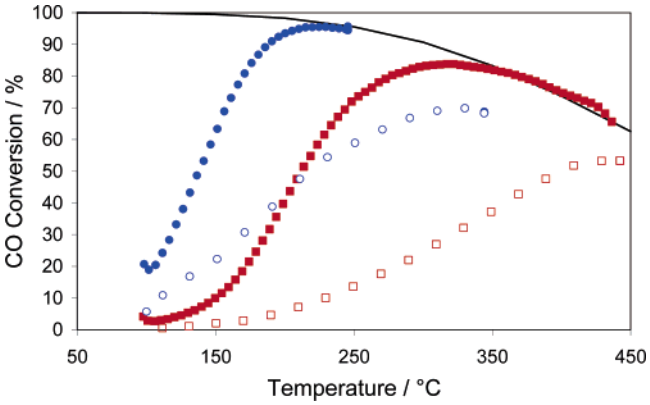

Figure 2. Catalytic activity under WGS conditions (2.0% CO, 2.5% CO_2, 7.5% H_2O, and 8.1% H_2 in N_2) for fresh 2% $Au/CeZrO_4$ ramped (blue filled circles), 2% $Au/CeZrO_4$ preexposed to WGS mixture at 350 °C (blue open circles), fresh 0.2% $Au/CeZrO_4$ ramped (red filled squares), 0.2% $Au/CeZrO_4$ preexposed to WGS mixture at 350 °C (red open squares). Full line shows the thermodynamic equilibrium conversion.

one under the conditions used in this study. At temperatures as low as 100 °C, 20% of the initial CO was converted to CO_2 and H_2, and, at 220−225 °C, equilibrium conversion was reached. Surprisingly high activity was also found for 0.2% $Au/CeZrO_4$, 50% conversion was found at 210 °C. In comparison the 2% Au/CeO_2 showed only 4% CO conversion at 200 °C and the equilibrium conversion was only achieved at 450 °C. Changing the active metal to platinum did increase the activity with the equilibrium conversion reached at 325 °C. Lower WGS activity was found for 2% Au/TiO_2 with only 8% CO conversion obtained at 450 °C. As expected, the oxide supports were not active for the WGS reaction in the temperature range investigated.

Figure 2 shows the effect of cycling the temperature under WGS over the 2 and 0.2% $Au/CeZrO_4$ catalysts. For both catalysts, the activity was stable after several cycles from 100 to 250 °C (up to three consecutive cycles were performed), and the catalytic activity remained after prolonged exposure to the WGS mixture at 250 °C. However, on increasing the WGS reaction temperature to 350 °C, significant deactivation was observed on repeating the temperature ramp. Prior to deactivation T(50%) was 130 °C, whereas, after the treatment at 350 °C, T(50%) increased to 210 °C for the 2% $Au/CeZrO_4$ catalyst. For the lower loaded catalyst, the T(50%) increased from 210

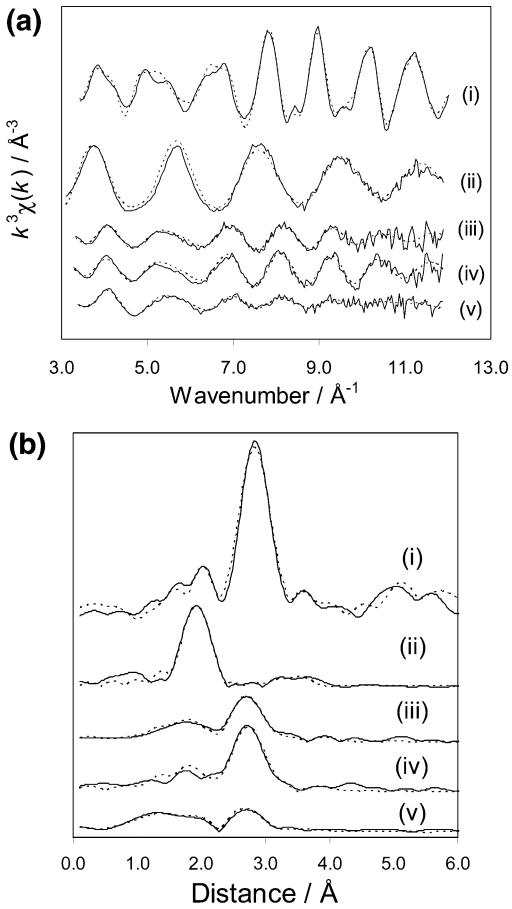

Figure 3. Comparison of the experimental (solid line) and fitted (dashed line) (a) Au L_{III} EXAFS and (b) pseudo radial distribution functions of (i) Au foil and the 2% $Au/CeZrO_4$ catalyst, (ii) as-received at room temperature, (iii) under WGS reaction conditions at 100 °C, (iv) after exposure to WGS conditions at 350 °C with the data recorded under WGS at 100 °C, and (v) following oxidation in air at 150 °C after reaction under WGS conditions at 100 °C.

to 398 °C. Furthermore, the equilibrium conversion could not be attained in the temperature range investigated.

In Situ EXAFS and XANES. Figure 3 shows the Au L_{III} EXAFS and the pseudo radial distribution functions of the 2% $Au/CeZrO_4$ catalyst for the fresh as-received catalyst, while exposed to the in situ WGS reaction mixture at 100 and 350 °C and under 20% O_2 at 150 °C after exposure to the WGS conditions at 100 °C. Table 3 summarizes the fitting parameters used for the EXAFS data under these conditions. Clearly, the fresh catalyst is dominated by the presence of oxygen coordination at ~2 Å, which is consistent with bond distances found in a gold oxide, such as Au_2O_3. (Note, however, that this should not be taken to imply that a crystalline oxide of gold is present; see later.)

Additional features at 3−4 Å are also found which have been fitted to cerium coordination in the second shell. It should be noted that although Au···Au distances in Au_2O_3 also occur at ~3.3 Å, the EXAFS data of the fresh catalyst could not be fitted with a Au in the second shell, either as a separate shell or a mixed shell. Scanning transmission electron microscopy (STEM) results on these catalysts show isolated gold atoms; however, a few gold-containing clusters (<1 nm) are also observed on the as-prepared catalyst.[37] These may be oxidized gold, but this could not be determined from the microscopy.

Under the WGS reaction, the data show only Au−Au distances at 2.76 and 3.80 Å. There are no detectable Au−O distances, indicating that the gold present is in the Au^0 state. Both first- and second-shell distances are shorter than in bulk gold, which is consistent with a high dispersion of gold in the sample. This is also consistent with the small first-shell coordination of 6.6 compared with 12 expected from large particles. Depending on whether spherical or hemispherical particles are present, the EXAFS data are consistent with an average particle size between 0.9 and 1.3 nm. The corresponding XANES data are shown in Figure 4 and are consistent with the EXAFS data, i.e. that virtually complete reduction from Au^{3+}, in the fresh catalyst, to Au^0 occurs at 100 °C under the WGS conditions. With increasing reaction temperature little change is observed in either the EXAFS or the XANES. Although this is not unexpected for the oxidation state, it is significant to note that no agglomeration of the metal particles is observed and the first-shell coordination remains between 6 and 7, even on heating the catalyst to 450 °C under WGS conditions.

On exposure to air at 150 °C following WGS at 100 °C, significant reoxidation takes place as clearly seen in both the EXAFS and XANES data. A Au−O distance at 1.97 Å can be fitted, and XANES shows an increase in the white line associated with cationic gold. Using linear combinations of the fresh catalyst as a "fully oxidized" sample and that under WGS as a "fully reduced" catalyst, we estimate that about 15% of the gold may be reoxidized under these conditions. Exposure to WGS conditions at 350 °C followed by exposure to air at 150 °C results in similar XANES data but with a smaller white-line intensity, indicating that less gold can be reoxidized after exposure to the reaction conditions at higher temperatures. After the WGS reaction at 350 °C, <5% of the gold was present in an oxidized state.

The Au L_{III} X-ray absorption data for the 0.2% $Au/CeZrO_4$ catalyst was also taken; however, due to the poor signal-to-noise ratio only XANES information was obtained. As found for the 2% $Au/CeZrO_4$ catalyst, the XANES data (see Figure 5) shows that much of the gold under WGS conditions is reduced and that although reoxidation is possible following reduction, this decreases with increasing WGS reaction temperature. A greater *proportion* of the gold can be oxidized in the case of the 0.2% $Au/CeZrO_4$ catalyst compared with the 2% $Au/CeZrO_4$ sample with 22% of the gold capable of being reoxidized following WGS at 100 °C and only 7% after reaction at 350 °C. All the estimations from the XANES are ±3%.

DFT Results. Five potential structures for the adsorption site of gold on $CeO_2(111)$ and (110) were calculated and fully optimized, shown in the Supporting Information, and selected structural details are summarized in Tables 4 and 5, respectively. For the adsorption of Au on a perfect $CeO_2(111)$, a Au atom was placed on the top of an oxygen atom and forms a short Au−O bond with a long Au−Ce distance consistent with a recent DFT study of Liu et al.[45] This binding of the gold is reasonably strong; however, in comparison, the substitution of a Au atom in an oxygen vacancy or in a cerium vacancy on $CeO_2(111)$ or $CeO_2(110)$ showed higher stability. The chemisorption energies of Au on both $CeO_2(111)$ and (110) are in the following order: E_{ad}(Ce-vacancy) > E_{ad}(O-vacancy) > E_{ad} (perfect-surface). It can be seen from Tables 4 and 5 that the average distances of Au−O are similar to those of Au−Ce if the Au is on the O vacancy on both $CeO_2(111)$ and (110): They are *all* around 3 Å. On the other hand, the average distances of Au−O are quite different from those of Au−Ce when Au is on the Ce-vacancy: On $CeO_2(110)$, the average distance of Au−O is 2.106 Å which is considerably shorter than that of Au−Ce (3.527 Å). The corresponding distances on $CeO_2(111)$ are significantly longer (over 10%).

TABLE 3: Structural Parameters from the Fitted EXAFS Spectra for 2% Au/$CeZrO_4$ As-Received, under WGS Conditions at 100 and 350 °C and after Reoxidation in Air at 150 °C Following Exposure to WGS at 100 °C (First- and Second-Shell Parameters for the Gold Foil Data Shown for Comparison)

catalyst	atom	shell distance[a]/Å	coordination no.[b]	Debye−Waller factor[c]/Å^2	fit factor/%
as received	O	1.98	3.6	0.007	21.9
	Ce	3.35	4.0	0.059	
in situ WGS 100 °C	Au	2.76	6.6	0.029	40.1
	Au	3.80	0.4	0.012	
in situ WGS 350 °C	Au	2.77	6.0	0.022	37.5
	Au	3.76	0.3	0.005	
in situ WGS 100 °C + air	O	1.97	0.5	0.022	43.4
	Au	2.75	7.0	0.044	
Au foil	Au	2.88	12	0.015	19.1
	Au	4.04	6	0.018	

[a] Estimated error ±0.1 Å. [b] Estimated error ±1. [c] Estimated error ±20%.

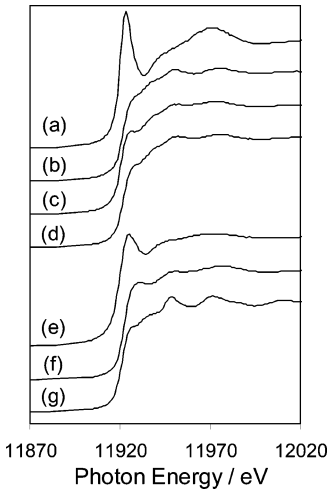

Figure 4. XANES spectra of the 2% Au/$CeZrO_4$ catalyst: (a) as-received catalyst at room temperature, (b) under WGS reaction conditions at 100 °C, and following oxidation in air at 150 °C after reaction under WGS conditions at (c) 100 and (d) 350 °C. Traces e−g correspond to the XANES from the standards Au_2O_3, $AuCl(PPh_3)_2$, and Au foil, respectively

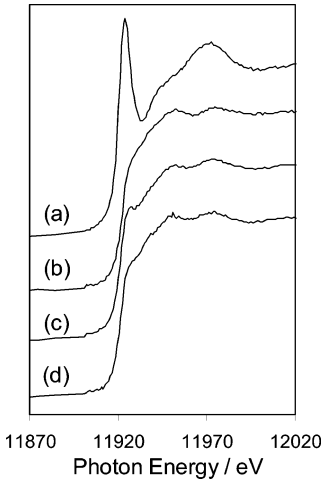

Figure 5. XANES spectra of the 0.2% Au/$CeZrO_4$ catalyst: (a) as-received catalyst at room temperature, (b) under WGS reaction conditions at 100 °C, and following oxidation in air at 150 °C after reaction under WGS conditions at (c) 100 and (d) 350 °C.

Discussion

Our DFT calculations for gold adsorbed on oxygen vacancies in $CeO_2(111)$ show that this is a more stable state than gold adsorbed on a perfect surface and is consistent with the very recent DFT calculations by Lui et al.[45] However, when we extend these calculations to include adsorption at *a cerium vacancy site*, we find that this further increases the chemisorption energy, indicating an even more favorable geometry for gold at a cation site as compared with gold at an anion site. Furthermore, the structure of gold adsorbed on the oxygen vacancy site for either the (111) or (110) surface does not agree with our experimental EXAFS or XANES data. The gold would be negatively charged on the oxygen vacancy, while the XANES data clearly show that the gold is strongly positively charged.

TABLE 4: Structural Parameters of Au on $CeO_2(111)$

structure	distance	av distance/Å
Au on the perfect surface (atop site of oxygen)	Au−O	2.051
	Au−Ce	3.785
Au on oxygen vacancy	Au−O	3.471
	Au−Ce	3.140
Au on cerium vacancy	Au−O	2.333
	Au−Ce	3.883

TABLE 5: Structural Parameters of Au on $CeO_2(110)$[a]

structure	distance	av distance/Å
Au on oxygen vacancy	Au-O	2.905
	Au-Ce	3.128
Au on cerium vacancy	Au-O	2.106
	Au-Ce	3.527

[a] It should be noted that, in the structure of Au on a cerium vacancy, an O atom near the Au is removed because it is less stable compared to the gas phase.

Comparing the DFT calculations reported herein with the experimental structure and XANES data indicates a consistency whereby the metal substitutes for a lattice cerium ion in the (110) surface and the surrounding oxygen atoms stabilize the positive charge on the gold. The fact that this occurs on the (110) surface and not that of (111) may indicate that the ceria particles in the catalysts are highly facetted, perhaps due to the small ceria particle size; the XRD of these catalysts shows an average ceria particle size of ∼6 nm. It should be noted that similar EXAFS data were obtained using a 2% Au/CeO_2 catalyst both in the fresh and under WGS conditions (see Supporting Information), and it is not thought that the role of the zirconium alters the state of the gold to any great extent. Therefore, the use of a CeO_2 support is a reasonable analogue for the mixed metal oxide support in order to model the gold structure. From the reaction data, it is clear that the support has a significant effect on the activity of the catalyst, with the addition of zirconia into the ceria lattice decreasing the light-off temperature. Preliminary DFT calculations have indicated that the presence of oxygen defects surrounding the metal particles are critical in the reaction mechanism. It is probable that the presence of zirconium in the oxide support stabilized these defects and thus promotes the catalysis. This view is in agreement with studies

on other noble metal catalysts supported on ceria−zirconia. For example Bozo et al. also postulated that the activation of the oxygen vacancies was the main reason for higher activity of mixed oxide support as opposed to changes in the metal structure.[46]

Actually, the reduction of the gold under WGS conditions is not surprising because both hydrogen and carbon monoxide are powerful reducing agents. This transformation is clearly demonstrated by the rapid color change of the catalyst and the exotherm generated on exposure to WGS conditions due to the ceria lattice becoming reduced. Although we cannot exclude the possibility of some residual oxidized gold under reaction conditions for these catalysts, the upper limit from the XANES data is 5%, and probably significantly less. The reduction of the support will decrease the stabilization of the gold in an oxidized form and, although some gold may remain in the lattice, the oxidation state will be reduced. Without the oxygen environment, it is likely that the gold would be very mobile and this would lead to the formation of nanoparticles. The formation of gold nanoparticles under reducing conditions has been observed on a number of catalysts, and similar particle sizes have been reported.[47] For example, Chao et al. demonstrated that 1 nm gold particles could be stabilized on mesoporous silica SBA-15 even after reduction with hydrogen at 300 °C.[48] In addition, 5% Au/TiO_2 has been examined as a function of reduction temperature and no sintering is found between room temperature and 200 °C, with a first-shell coordination number between 7 and 8.[49]

The formation of the nanoparticles is thought to be seeded at gold atoms embedded in the lattice. On both CeO_2 and TiO_2, DFT calculations indicate that gold binds to these sites, forming small particles strongly interacting with the oxide support.[45,50] In comparison, the binding of gold to the clean oxide surface is less favorable than metallic bonding and results in gold particles which do not wet the surface. The strong wetting of the gold particles is supported by our experimental results, following reoxidation of the catalyst in air at 150 °C. Surprisingly, although the metal is reduced even under mild reaction conditions, a significant proportion of the gold is reoxidizable. This may be understood by a reoxidation of the support which stabilizes the cationic gold in the lattice again. Only partial reoxidation is possible because the majority of gold atoms are not in contact with the support: in 1.3 nm hemispherical particles approximately 15% of the atoms are directly connected to the support. This is comparable with the amount oxidizable by air and may indicate that all the gold bound to the surface of the ceria at the gold particle/support interface can be reoxidized by exposure to air at 150 °C. No significant redispersion of the gold is found on reoxidation as indicated by the EXAFS data.

The reoxidation results can be used to understand the catalytic activity data and the effect of temperature on the stability of the catalyst under the WGS conditions. Although the 2% $Au/CeZrO_4$ has very good low-temperature activity, this is lost if the temperature exceeds 250 °C. Coincident with the loss of activity, the proportion of the reoxidizable gold is reduced significantly. In contrast, when exposed to the WGS conditions, the EXAFS data clearly show that after reduction the average gold particle size is independent of the reaction conditions, indicating that the deactivation observed after exposure to WGS conditions at 350 °C is not due to metal phase sintering. One possible explanation for the EXAFS, XANES, and activity data as a function of temperature is that, on heating to a high temperature, the gold stabilized in the lattice of the ceria becomes detached from the lattice vacancy. The nanoparticle is no longer anchored via a cationic gold adatom, and the binding with the surface decreases. This also means that the intimate contact between the support and the gold particle, which governs the redox properties of the support and the adsorptive properties of the gold particles is diminished and the low-temperature WGS activity is lost. This is in agreement with many studies which show that the formation and maintenance of the metal/support interaction is critical if the gold is to remain active. A similar structure was proposed for gold catalysts active for CO oxidation, whereby the gold cations act as a "chemical glue" between the gold nanoparticle and the oxide support.[51]

The proposed deactivation process that is attributed to "dewetting" of the support deactivation process is not in agreement with the explanation proposed by Kim and Thompson.[28] Using XPS and IR to characterize both fresh and deactivated Au/CeO_2 catalysts, they concluded that the deactivation was caused primarily by blockage of the active sites by carbonate and/or formate species. However, in contrast to our catalysts, their catalyst showed the presence of gold in a relatively high oxidation state for both the fresh and the deactivated catalysts, and this may explain the difference in the conclusions.

Although the lattice-stabilized ionic gold *in the fresh catalyst* is consistent with the model proposed by Flytzani-Stephanopoulos and co-workers.,[27,34,35] the catalysts reported herein differ significantly from those prepared in their work both in terms of activity (our catalysts are very much more active at low temperatures) and the oxidation state of the gold under reaction conditions. Flytzani-Stephanopoulos et al. described a mechanism based on cationic gold active sites and where gold nanoparticles are spectators; however, under our conditions this is unlikely. All the catalysts showed clear evidence for metallic gold under WGS conditions even for the 0.2 wt % loading, which indicates that if cationic gold was responsible for the activity of our catalysts, the number of active sites would be very small and the turnover number would have to be exceptionally high. We think this is unlikely.

Conclusions

A combined experimental and computational investigation of gold catalysts that are found to be exceptionally active for the water gas shift reaction leads to the conclusion that the active form of gold is metallic. Both the EXAFS and XANES experimental results and the DFT calculations point to a model in which a metallic gold cluster containing about 50 atoms is in intimate contact with the oxide support to the extent that up to 15% of the gold "atoms" at the interface with the support may be located at cation vacancies. Such gold atoms would be expected to carry a small positive charge ($Au^{\delta+}$), and this may be very important for creating the active site for the water gas shift reaction. However, it is clear that *metallic* gold particles rather than isolated gold ions (e.g. Au^{3+}) are present under reaction conditions. We conclude that metallic gold in close contact with the oxide support provides the active sites for the water gas shift reaction on these very active catalysts.

Acknowledgment. We acknowledge CCLRC for EXAFS beam time and EPSRC for funding under the CARMAC project.

Supporting Information Available: Fitting parameters, EXAFS, and pseudo radial distribution functions of the 2% Au/CeO_2 catalyst both fresh and under WGS conditions at 100 °C.

Optimized structures and positions used in the DFT calculations for the gold adsorption on CeO_2(111) and CeO_2(110). This material is available free of charge via the Internet at http://pubs.acs.org.

References and Notes

(1) Cameron, D.; Holliday, R.; Thompson, D. T. *J. Power Sources* **2003**, *118*, 298.

(2) Haruta, M.; Kobayachi, T.; Sano, H.; Yamada, N. *Chem. Lett.* **1987**, 405.

(3) Haruta, M.; Yamada, N.; Kobayachi, T.; Iijima, S. *J. Catal.* **1989**, *115*, 301.

(4) Bond, G. C.; Thompson, D. T. *Catal. Rev.−Sci. Eng.* **1999**, *41*, 319.

(5) Trimm, D. L.; Onsan, Z. I. *Catal. Rev.−Sci. Eng.* **2001**, *43*, 31.

(6) Pattrick, G.; Van Der Linger, E.; Corti, C. W.; Thompson, D. T. *Top. Catal.* **2004**, *30−31*, 273.

(7) Andreeva, D. *Gold Bull.* **2002**, *35*, 82.

(8) Haruta, M.; Daté, M. *Appl. Catal., A* **2001**, *222*, 427.

(9) Daniells, S. T.; Makkee, M.; Moulijn, J. A. *Catal. Lett.* **2005**, *100*, 39.

(10) Hua, J. M.; Wei, K. M.; Zheng, Q.; Lin, X. G. *Appl. Catal., A* **2004**, *259*, 121.

(11) Venugopal, A.; Scurrell, M. S. *Appl. Catal., A* **2004**, *258*, 241.

(12) Kozlov, A. I.; Kozlova, A. P.; Asakura, K.; Matsui, Y.; Kogure, T.; Shido, T.; Iwasawa, Y. *J. Catal.* **2000**, *196*, 56.

(13) Andreeva, D.; Tabakova, T.; Idatiev, V.; Christov, D.; Giovanoli, R. *Appl. Catal., A* **1998**, *169*, 9.

(14) Ilieva, L. I.; Andreeva, D. H.; Andreev, A. A. *Thermochim. Acta* **1997**, *292*, 169.

(15) Andreeva, D.; Idakiev, V.; Tabakova, T.; Andreev, A. *J. Catal.* **1996**, *158*, 354.

(16) Luengnaruemitchai, A.; Osuwan, S.; Gulari, E. *Catal. Commun.* **2003**, *4*, 215.

(17) Andreeva, D.; Idakiev, V.; Tabakova, T.; Andreev, A.; Giovaloni, R. *Appl. Catal., A* **1996**, *134*, 275.

(18) Tabakova, T.; Idakiev, V.; Andreeva, D.; Mitov, I. *Appl. Catal., A* **2000**, *202*, 91.

(19) Boccuzzi, F.; Chiorino, A.; Andreeva, D.; Tabakova, T. *J. Catal.* **1999**, *188*, 176.

(20) Idakiev, V.; Yuan, Z. Y.; Tabakova, T.; Su, B. L. *Appl. Catal., A* **2005**, *281*, 149.

(21) Boccuzzi, F.; Chiorino, A.; Manzoli, M.; Andreeva, D.; Tabakova, T.; Ilieva, L.; Idakiev, V. *Catal. Today* **2002**, *75*, 169.

(22) Valden, M.; Lui, X.; Goodman, D. W. *Science* **1998**, *281*, 1647.

(23) Sakurai, H.; Veda, A.; Kobayashi, T.; Haruta, M. *Chem. Commun.* **1997**, 271

(24) Idakiev, V.; Tabakova, T.; Yuan, Z. Y.; Su, B. L. *Appl. Catal., A* **2004**, *270*, 135.

(25) Mohamed, M. M.; Salama, T. M.; Ishikawa, M. *J. Colloid Interface Sci.* **2000**, *224*, 366.

(26) Venugopal, A.; Scurrell, M. S. *Appl. Catal., A* **2004**, *258*, 241.

(27) Fu, Q.; Deng, W.; Saltsburg, H.; Flytzani-Stephanopoulos, M. *Appl. Catal., B* **2005**, *56*, 57.

(28) Kim, C. H.; Thompson, L. T. *J. Catal.* **2005**, *230*, 66.

(29) Andreeva, D.; Idakiev, V.; Tabakova, T.; Ilieva, L.; Falaras, P.; Bourlinos, A.; Travlos, A. *Catal. Today* **2002**, *72*, 51.

(30) Tabakova, T.; Boccuzzi, F.; Manzoli, M.; Sobczak, J. W.; Idakiev, V.; Andreeva, D. *Appl. Catal., B* **2004**, *49*, 73.

(31) Jacobs, G.; Patterson, P. M.; Williams, L.; Chenu, E.; Sparks, D.; Thomas, G.; Davis, B. H. *Appl. Catal., A* **2004**, *262*, 177.

(32) Tabakova, T.; Boccuzzi, F.; Manzoli, M.; Andreeva, D. *Appl. Catal., A* **2003**, *252*, 385.

(33) Fu, Q.; Weber, A.; Flytzani-Stephanopoulos, M. *Catal. Lett.* **2001**, *77*, 87.

(34) Fu, Q.; Salzburg, H.; Flytzani-Stephanopoulos, M. *Science* **2003**, *301*, 935.

(35) Fu, Q.; Kudriavtseva, S.; Saltzburg, H.; Flytzani-Stephanopoulos, M. *Chem. Eng. J.* **2003**, *93*, 41.

(36) Jacobs, G.; Chenu, E.; Patterson, P. M.; Williams, L.; Sparks, D.; Thomas, G.; Davis, B. H. *Appl. Catal., A* **2004**, *258*, 203.

(37) Amieiro Foncesca, A.; Fisher, J.; Thompsett, D. Unpublished results.

(38) Haruta, M. *Gold Bull.* **2004**, *37*, 27.

(39) Venezia, A. M.; Pantaleo, G.; Longo, A.; Di Carlo, G. D.; Casaletto, M. P.; Liotta, F. L.; Deganello, G. *J. Phys. Chem. B* **2005**, *109*, 2821.

(40) Goguet, A.; Meunier, F.; Breen, J. P.; Burch R.; Petch, M. I.; Faur Ghenciu, A. *J. Catal.* **2004**, *226*, 382.

(41) Binstead, N. EXCURV98, CCLRC Daresbury Laboratory computer program, 1998.

(42) (a) Perdew, J. P.; Chevary, J. A.; Vosko, S. H.; Jackson, K. A.; Pederson, M. R.; Singh, D. J.; Fiolhais, C. *Phys. Rev. B* **1992**, *46*, 6671. (b) Vanderbilt, D. *Phys. Rev. B* **1990**, *41*, 7892.

(43) (a) Eyring, L. In *Handbook on the Physics and Chemistry of Rare Earths*; Gschneider, K. A., Eyring, L., Eds.; North-Holland: Amsterdam, 1979. (b) Wyckoff, R. W. G.; Wollan, E. O. *Acta Crystallogr.* **1953**, *6*, 741.

(44) (a) Skorodumovaetal, N. V.; Ahuja, R.; Simak, S. I.; Abrikosov, I. A.; Johansson, B.; Lundqvist, B. I. *Phys. Rev. B* **2001**, *64*, 115108. (b) Yang, Z.; Woo, T. K.; Baudin, M.; Hermansson, K. *J. Chem. Phys.* **2004**, *120*, 7741.

(45) Liu, Z.-P.; Jenkins, S. J.; King, D. A. *Phys. Rev. Lett.* **2005**, *94*, 196102.

(46) Bozo, C.; Guilhaume, N.; Herrmann J.-M. *J. Catal.* **2001**, *203*, 393.

(47) (a) Calla, J. T.; Davis, R. J. *J. Phys. Chem. B* **2005**, *109*, 2307. (b) Calla, J. T.; Davis, R. J. *Catal. Lett.* **2005**, *99*, 21.

(48) Chao, K.-J.; Cheng, M.-H.; Ho, Y.-F.; Liu, P.-H. *Catal. Today* **2004**, *97*, 49.

(49) Schwartz, V.; Mullins, D. R.; Yan, W.; Chen, B.; Dai, S.; Overbury S. H. *J. Phys. Chem. B* **2004**, *108*, 15782.

(50) Lopez, N.; Nørskov, J. K.; Janssens, T. V. W.; Carlsson, A.; Puig-Molina, A.; Clausen, B. S.; Grunwaldt, J.-D. *J. Catal.* **2004**, *225*, 86.

(51) Bond, G. C.; Thompson, D. T. *Gold Bull.* **2000**, *33*, 41.